Determination of dust aerosol particle size at Gale Crater using REMS UVS and Mastcam measurements

Álvaro Vicente-Retortillo[1,2], Germán M. Martínez[2], Nilton O. Renno[2], Mark T. Lemmon[3] and Manuel de la Torre-Juárez[4]

[1]Departamento de Física de la Tierra, Astronomía y Astrofísica II, Universidad Complutense de Madrid, Madrid, Spain

[2]Department of Climate and Space Sciences and Engineering, University of Michigan, Ann Arbor, Michigan, USA.

[3]Department of Atmospheric Sciences, Texas A&M University, College Station, Texas, USA

[4]Jet Propulsion Laboratory, California Institute of Technology, Pasadena, California, USA.

Corresponding author: Álvaro Vicente-Retortillo (alvarodv@ucm.es)

Key Points:

- We have developed a novel methodology to retrieve dust aerosol particle size at Gale Crater using Mars Science Laboratory data
- The retrieved dust effective radii range from 0.6 μm during the clear aphelion season to 2 μm during the dusty perihelion season
- Our results improve the estimation of ultraviolet radiation fluxes at the Martian surface

This is the author manuscript accepted for publication and has undergone full peer review but has not been through the copyediting, typesetting, pagination and proofreading process, which may lead to differences between this version and the Version of Record. Please cite this article as doi: 10.1002/2017GL072589

Abstract

We calculate the seasonal and interannual variation in dust aerosol particle size above Gale Crater during the first 1413 sols of the Mars Science Laboratory (MSL) mission. Measurements of UV radiation made by the Rover Environmental Monitoring Station (REMS) in combination with atmospheric opacities retrieved from the Mastcam instrument are used for the calculations. Our results indicate that the dust effective radius varies significantly with season, ranging from ~0.6 μm during the low opacity season (L_s = 60º – 140º) to ~2 μm during the high opacity season (L_s = 180º – 360º). Our results suggest that Gale Crater is affected by dust events of high aerosol content originated at various distances from it. Our results improve the accuracy of estimations of ultraviolet radiation fluxes at the Martian surface. Moreover, our results have important implications because the lifetime of suspended dust and its ability to nucleate clouds are affected by particle size.

1. Introduction

Dust is ubiquitous in the Martian atmosphere and interacts strongly with solar and thermal radiation [*Read and Lewis*, 2004]. In particular, dust particle size determines the ratio between the atmospheric opacity at short and long wavelengths, affecting heating rates and influencing the thermal and dynamical structure of the Martian atmosphere [*Kahre et al.*, 2008; *Madeleine et al.*, 2011; *Medvedev et al.*, 2011]. Moreover, dust particle size strongly influences atmospheric transport and gravitational settling rates [*Kahre et al.*, 2008].

The Mars Science Laboratory (MSL) Curiosity rover landed at 4.6ºS and has been operating for more than two Martian years. Curiosity is equipped with environmental and remote sensing science instruments [*Grotzinger et al.*, 2012] capable of providing insight into the size of atmospheric aerosols. In particular, the Rover Environmental Monitoring Station (REMS) contains a UV sensor (UVS) that has been measuring solar radiation at the surface of Mars for the first time in six bands between 200 and 380 nm [*Gómez-Elvira et al.*, 2012], while observations from the Mast Camera (Mastcam) instrument have been used to retrieve atmospheric dust opacity from direct images of the Sun at the wavelengths of 440 and 880 nm [*Smith et al.*, 2016].

In Section 2, we present a novel methodology to determine dust particle sizes using REMS/UVS measurements in combination with Mastcam retrievals of atmospheric opacity. In Section 3, we show the retrieved values of the dust particle size and analyze its seasonal and interannual variability during the first 1413 sols (Martian days) of the MSL mission. In Section 4, we discuss the impact of atmospheric circulations at Gale Crater on the relationship between atmospheric opacity and dust particle sizes. We also discuss the seasonal evolution of the UV radiation at Gale Crater and the impact of particle size on it. Finally, in Section 5 we summarize the main results of our study.

2. Methodology

2.1 Data Selection

The REMS/UVS nominal strategy for data acquisition consists of 5 minutes of measurements at 1 Hz every hour, with at least an additional hour of measurements at 1 Hz during each sol [*Gómez-Elvira et al.*, 2014], while the Mastcam nominal strategy for atmospheric opacity retrievals consists of measurements made every three to seven sols [*Smith et al*., 2016].

This study uses the photodiode output currents (stored as TELRDR products in the NASA Planetary Data System (PDS)) of the REMS/UVS UVE channel (300-350 nm), the ancillary data records (ADR) containing the geometry of the rover and the Sun, and the values of the atmospheric opacity at the reference wavelength of 880 nm retrieved from the Mastcam measurements. The UVE channel is selected for this study because it matches the 320 nm UV channel of the Mars Color Imager (MARCI) onboard the Mars Reconnaissance Orbiter (MRO), from which the refractive indices that we use in the calculations of the radiative properties of the dust particles are obtained [*Wolff et al*., 2010].

We use UVS TELRDR measurements conducted when the Sun is temporarily blocked by the masthead or the mast of the rover because values of the photodiode output currents depend on the dust aerosol particle size during these shadow events. As the Sun moves towards the edge of the blocked region of the field of view (FOV), the relative change in the irradiance measured by the UVS decreases with decreasing aerosol particle size. This effect is illustrated in Figure S1 (see Supporting Information). In order to accurately calculate the fraction of the incoming radiation that is blocked, we use only UVS TELRDR measurements made when the masthead is in its most typical position (azimuth ~ -179º and elevation ~ 43º).

2.2 Calculation of Radiative Properties and Radiances

Dust radiative properties, in particular single scattering albedo and scattering phase function, are key to determine radiation at the surface accurately. These two parameters depend on the refractive indices, the shape, and the size distribution of the dust particles. We calculate the single scattering albedo and scattering phase function using a T-Matrix code [*Mishchenko and Travis*, 1998], assuming that particles are cylinders with diameter-to-length ratio D/L = 1 [*Wolff et al*., 2009] that follow a power law distribution [*Hansen and Travis*, 1974; *Mishchenko and Travis*, 1994] with a typical effective variance of 0.3 [*Rannou et al.*, 2006; *Madeleine et al*., 2011]. Next, we simulate the hemispherical UV radiance at the surface during shadow events using a Monte-Carlo radiative transfer scheme. UV fluxes and radiances simulated using this scheme are in excellent agreement with those estimated using the COMIMART and DISORT models [*Vicente-Retortillo et al*., 2015; *Stamnes et al.*, 1988]. Details on our Monte-Carlo model and its validation are provided in the Supporting Information (Texts S1 and S2, and Figure S2).

2.3 Simulation of the Photodiode Output Current

We calculate the photodiode output current using the simulated UV radiance and an empirical model that considers the tilt and orientation of the rover, the angular response of the photodiode as a function of the zenith angle (θ), and the region of the FOV blocked by the masthead and the mast.

The empirical angular response of the UVE channel obtained using TELRDR and ADR products is shown in the left panel of Figure 1. The angular response used to obtain processed UV fluxes (in units of Wm^{-2}, stored as ENVRDR products in the NASA PDS) from the TELRDR products is shown for comparison. Our empirically derived calibration function differs from the one used to produce the ENVRDR products. Thus, for physical consistency, we use the photodiode output currents (TELRDR products) and the empirical angular response in our calculations instead of the processed UV fluxes (ENVRDR products).

The empirically derived blocked region of the FOV is shown in the right panel of Figure 1. The black line represents the trajectory of the Sun across the FOV on sol 1362, the red dots represent REMS measurement sessions and the green dots represent the selected shadow event.

2.4 Particle Size Retrieval

We use UVS TELRDR measurements covering the full duration of each shadow event. For each of these measurements, we simulate the output currents (S) as a function of the effective radius as

$$S = \sum_{i=1}^{N} L_i \cdot \mu_i \cdot R_i \cdot F_i \cdot \Omega_i,$$

where L is the simulated radiance, μ is the cosine of the zenith angle, R is the value of the normalized angular response, F indicates whether the incoming radiance is blocked (F = 0) or not (F = 1), Ω is the solid angle, and i denotes each of the $N = 360^2$ grid cells separated by 0.25º in zenith angle and by 1º in azimuth. The computed radiances are stored in a 5-D lookup table as a function of opacity, solar zenith angle and dust aerosol effective radius.

Then, the ratios between the output currents as the Sun moves towards the edge of the blocked region of the FOV, simulated as a function of the dust aerosol effective radius, are calculated. From these simulated ratios, we determine the radii that best match the measured ratios. Finally, for each solar longitude (L_s) and Martian year, we calculate the mean and the standard deviation of the corresponding retrieved radii. Error bars in Figures 2 and 3 represent these standard deviations.

Our estimations of the dust aerosol effective radii are robust to changes in dust opacity. To illustrate this, we select sol 1362 (when the atmospheric opacity (τ) was ~0.7 and the dust particle size that we retrieve is slightly above 1.5 μm). Table 1 shows that when r_{eff} = 1.5 μm, underestimated and overestimated opacities of 0.5 and 1.0 lead to departures of only -0.4% and 4% in the simulated ratio with respect to the observed ratio, which in turn result in changes of the

retrieved effective radii of only -4% and 6%, respectively (not shown in the table). Discrepancies between observed and simulated ratios are significantly larger for the other considered radii, showing that the ratio between output currents during a shadow event is a suitable parameter to retrieve dust particle sizes (Section 2.1). Further evidence of the strong dependence of observed ratios on the dust particle size is given in the Supporting Information (Figure S3).

In this study, we have not considered the contribution of water ice clouds to atmospheric opacity. However, the impact of clouds on the retrieved value of dust particle sizes is generally small. As an example, we select a shadow event on sol 1280, when the total atmospheric opacity is around the annual minimum (L_s = 122º) and the water ice contribution to opacity is expected to be maximum [*Smith*, 2004]. Assuming that the fraction of opacity contributed by ice is 10%, 20%, 30% and 40%, we obtain increases in the retrieved effective radius below 3%, 9%, 18% and 28%, respectively. In Gale Crater, this fraction is typically below 20% except during the low opacity season (especially around L_s ~ 120º), when it can be in the range 30-40% [*McConnochie et al*., 2015]. The water ice radiative properties were determined using the refractive indices given by *Warren* [1984], assuming spherical particles with a size distribution characterized by an effective radius of 3 μm [*Wolff and Clancy*, 2003] and an effective variance of 0.1 [*Wolff and Clancy*, 2003; *Madeleine et al*., 2012].

Other sources of uncertainties include simulated radiances (which are mainly affected by the scattering phase function) and the empirically derived angular response. These and other sources of uncertainty are explained in detail in the Supporting Information (Text S3).

3. Results

The seasonal and interannual variability of the dust particle effective radius is shown in the top panel of Figure 2 as a function of L_s for MY 31 (blue), MY 32 (black) and MY 33 (red). Mastcam dust opacity values obtained using a running mean of 10 sols are shown in the bottom panel for comparison.

Dust particle size shows a significant seasonal variability, with values of the effective radius ranging from ~0.6 to ~2 μm. During the aphelion season (L_s = 0º – 180º), the dust particle size is relatively small, with an annual minimum of ~0.6 μm at L_s ~ 125º, coinciding with the lowest annual values of atmospheric opacity. During the perihelion season (L_s = 180º – 360º), the dust particle size is significantly larger with two relative maxima associated with periods of enhanced dust activity between L_s = 210º – 270º and L_s = 310º – 350º, and one relative minimum coinciding with a local minimum in the atmospheric opacity at L_s ~ 300º.

From an interannual perspective, the seasonal cycle of the dust aerosol particle size is similar from MY 31 to MY 33, although some differences exist. On one hand, dust effective radii during the low opacity season (L_s = 60º – 140º) in MY 33 are lower than in MY 32 (Figure 2, top). These differences could result from the combination of smaller dust particles and a larger contribution of water ice clouds to the total atmospheric opacity during the aphelion season of

MY 33, as the increase in water ice cloud fraction leads to an underestimation of the retrieved radii due to the changes in the aerosol radiative properties that are not being considered (Section 2.4). On the other hand, observed differences between MY 31 and 32 during the perihelion season are associated with interannual variability in the events of enhanced opacity (Figure 2, bottom).

Our results are consistent with those obtained for the Mars Exploration Rovers (MER) Spirit and Opportunity landing sites. At both MER locations, particle sizes were found to range from 0.7 to 2.1 μm, with the lowest values occurring during the low atmospheric opacity season, and the largest values generally occurring when the opacity peaks [*Lemmon et al*., 2015].

4. Discussion

4.1. Implications of atmospheric circulations on the correlation between opacity and dust particle size

Figure 3 shows the retrieved effective radii as a function of atmospheric opacity measured by Mastcam, with color code indicating L_s. The correlation between the two variables is apparent (R^2 = 0.67), especially during the aphelion season, when $\tau < 1$. This behavior is physically consistent because dust particles are expected to be smaller during the low atmospheric opacity season because larger particles lifted during dust events settle more rapidly than the smallest particles.

The lack of a clear correlation between atmospheric opacity and dust particle size during the perihelion season (when $\tau > 1$) suggests that Gale Crater is affected by dust events originated at various distances from the observation site (likely outside Gale Crater). The larger particle radii and smaller opacity of the events represented by the brown points suggest that they are associated with dust events originated closer to Gale Crater than the higher opacity and lower radii events represented by yellow-orange points because larger particles are expected to be deposited more rapidly during transport (smaller particles remain suspended for longer periods of time). This is further supported by strong and persistent northerly and northwesterly winds at Gale Crater during the perihelion season centered around L_s = 270º [*Rafkin et al.*, 2016]. The lack of correlation between atmospheric opacity and dust particle size at high opacity values has also been observed at the MER sites [*Lemmon et al*., 2015].

4.2. Implications of dust particle size on the UV environment

Quantification of the UV radiation at the Martian surface is important for assessing the habitability of the planet [*Córdoba-Jabonero et al.*, 2003]. The daily UV irradiation (defined as the total amount of solar energy received during one sol from the ultraviolet region of the spectrum) is of particular interest because of its effects on microorganisms [*Cockell and Raven*, 2004] and the correlation that appears to exist with variations in background methane concentrations measured at the MSL landing site [*Webster et al.*, 2016]. The daily UV irradiation

is controlled by the seasonal evolution of the solar radiation at the top of the atmosphere (TOA) and by the radiative properties of the atmosphere, in which dust particle size plays an important role.

The top panel of Figure 4 shows the seasonal evolution of the daily UV irradiation at the TOA and at the surface of Gale Crater, along with opacity values retrieved from Mastcam. To calculate the daily UV irradiation at the surface we use the COMIMART radiative transfer model [*Vicente-Retortillo et al.,* 2015] with retrieved Mastcam opacities at 880 nm and calculated dust particle effective radii shown in Figure 2 as inputs. In this model, these opacities are scaled to UV wavelengths using the ratio of the computed extinction efficiencies, calculated using the refractive indices obtained by *Wolff et al.* [2009] and *Wolff et al.* [2010], and which in turn depend on the retrieved effective radii. We consider the perihelion season of MY 32 and the aphelion season of MY 33 to cover one full Martian year. The highest values of the UV irradiation at the surface are found at L_s ~ 185º – 200º and L_s ~ 295º – 310º, when the UV irradiation at the TOA is relatively high and the atmospheric opacities are the lowest of the dusty season. The lowest annual values occur between L_s = 0º - 100º, when the radiation at the TOA is relatively low and its decrease toward the annual minimum is partially compensated by the decrease in opacity. Minimum values also occur at L_s ~ 230º, when the irradiation at the TOA is close to the maximum but the atmospheric opacity shows the highest annual values, and at L_s ~335º, when the second maximum in atmospheric opacity occurs.

In order to illustrate the impact of considering a variable particle size on the calculations of the ultraviolet radiation at the Martian surface, we show in the bottom panel of Figure 4 the ratio between the daily UV irradiation at the surface assuming a constant effective radius of 1.5 μm and that assuming a time-dependent size as shown in Figure 2. When the fixed effective radius of 1.5 μm is assumed, daily UV irradiations are underestimated during the low opacity season (L_s = 60º – 140º) and around the local minimum in opacity and effective radius at L_s ~ 300º, while they are overestimated during the periods of enhanced opacity (L_s = 210º – 270º and L_s ~ 335º), when particles are larger.

5. Conclusions

We have developed a novel methodology to calculate dust aerosol particle size at Gale Crater and analyzed its temporal variability during the first 1413 sols of the MSL mission. We have used measurements of UV radiation acquired at the Martian surface for the first time by the REMS UVS and atmospheric opacity values retrieved from the Mastcam instrument.

Dust aerosol particle size shows a significant seasonal variability, with effective radii ranging from ~0.6 to ~2 μm. The lowest values are found during the low opacity season, whereas the highest ones are typically associated with events of enhanced dust content. From an interannual perspective, the general behavior of the particle size evolution in MY 31-32 is similar to that in MY 32-33. During the low opacity season (L_s = 60º – 140º) in MY 33, the retrieved dust effective radii are significantly lower than in MY 32. A larger contribution of

water ice clouds to the total atmospheric opacity during the aphelion season of MY 33, which we have not considered in our calculations of the effective radii, can partially explain such a departure.

The correlation between atmospheric opacity and dust aerosol particle size is apparent during the aphelion season, when the atmospheric opacity is low. The lack of a clear correlation between both quantities during the perihelion dusty season suggests that Gale Crater is affected by dust events originating at various distances from the rover site.

The determination of dust aerosol particle size is important because it leads to improvements in the accuracy of calculations of the UV environment at the surface and aerosol atmospheric transport, including gravitational settling rates. In addition, it leads to improvements in predictions of atmospheric heating rates, which affect the atmospheric thermal and dynamical fields.

Acknowledgements

This study has been partially supported by the research projects AYA2011-29967-C05-02 and CGL2011-25327, funded by the Spanish Ministry of Economy and Competitiveness, and by JPL grant number 1449038. Also, the author A. Vicente-Retortillo wishes to acknowledge the Ministry FPI scholarship (BES-2012-059241) for the financial support and training. N.O. Renno acknowledges the support from the National Science Foundation via Award AGS 1526444. REMS TELRDR and ADR products can be found in the NASA PDS (http://atmos.nmsu.edu/PDS/data/mslrem_1001/DATA/).

References

Cockell, C.S. and J. A. Raven (2004), Zones of photosynthetic potential on Mars and the early Earth, *Icarus*, 169, 300-310, doi:10.1016/j.icarus.2003.12.024.

Córdoba-Jabonero, C., L.M. Lara, A.M. Mancho, A. Márquez, and R. Rodrigo (2003), Solar ultraviolet transfer in the Martian atmosphere: biological and geological implications, *Planet. Space Sci.*, 51, 399–410, doi: 10.1016/S0032-0633(03)00023-0.

Gómez-Elvira, J., et al. (2012), REMS: The Environmental Sensor Suite for the Mars Science Laboratory Rover, *Space Sci. Rev.*, 170, 583-640, doi:10.1007/s11214-012-9921-1.

Gómez-Elvira, J., et al. (2014), Curiosity's rover environmental monitoring station: Overview of the first 100 sols, *J. Geophys. Res. Planets*, 119, 1680–1688, doi:10.1002/2013JE004576.

Grotzinger, J.P., et al. (2012), Mars Science Laboratory Mission and Science Investigation, *Space Sci. Rev.*, 170, 5-56, doi:10.1007/s11214-012-9892-2.

Hansen, J.E., and L.D. Travis (1974), Light scattering in planetary atmospheres. *Space Sci. Rev.*, 16, 527–610.

Kahre, M.A., J.L. Hollinsworth, R.M. Haberle and J.R. Murphy (2008), Investigations of the variability of dust particle sizes in the martian atmosphere using the NASA Ames General Circulation Model, *Icarus*, 195, 576-597, doi: 10.1016/j.icarus.2008.01.023.

Lemmon, M.T., M.J. Wolff, J.F. Bell III, M.D. Smith, B.A. Cantor, and P.H. Smith (2015), Dust aerosol, clouds, and the atmospheric optical depth record over 5 Mars years of the Mars Exploration Rover mission, *Icarus*, 251, 96–111, doi: 10.1016/j.icarus.2014.03.029.

Madeleine, J.-B., F. Forget, E. Millour, L. Montabone, and M.J. Wolff (2011), Revisiting the radiative impact of dust on Mars using the LMD Global Climate Model. *J. Geophys. Res.*, 116, E11010, doi: 10.1029/2011JE003855.

Madeleine, J.-B., F. Forget, E. Millour, T. Navarro, and A. Spiga (2012), The influence of radiatively active water ice clouds on the Martian climate, *Geophys. Res. Lett.*, 39, L23202, doi: 10.1029/2012GL053564.

McConnochie, T.H., et al. (2015), ChemCam Passive Sky Spectroscopy at Gale Crater: Diurnal and Seasonal cycles of O2, H2O, and aerosols, presented at 2015 AGU Fall Meeting, San Francisco, California, USA.

Medvedev, A. S., T. Kuroda and P. Hartogh (2011), Influence of dust on the dynamics of the martian atmosphere above the first scale height, *Aeolian Res.*, 3(2), 145-156, doi: 10.1016/j.aeolia.2011.05.001.

Mishchenko, M. I., and L. D. Travis (1994), Light scattering by polydispersions of randomly oriented spheroids with sizes comparable to wavelengths of observation. *Appl. Opt.*, 33, 7206-7225, doi:10.1364/AO.33.007206.

Mishchenko, M. I., and L. D. Travis (1998), Capabilities and limitations of a current FORTRAN implementation of the T-matrix method for randomly oriented, rotationally symmetric scatterers. *J. Quant. Spectrosc. Radiat. Transfer*, 60, 309-324.

Rafkin, S.C.R., J. Pla-Garcia, M. Kahre, J. Gomez-Elvira, V. E. Hamilton, M. Marín, S. Navarro, J. Torres, A. Vasavada (2016), The meteorology of Gale Crater as determined from

Rover Environmental Monitoring Station observations and numerical modeling. Part II: Interpretation, *Icarus*, 280, 114-138, doi:10.1016/j.icarus.2016.01.031.

Rannou, P., S. Perrier, J.L. Bertaux, F. Montmessin, O. Korablev, and A. Rébérac (2006), Dust and cloud detection at the Mars limb with UV scattered sunlight with SPICAM. *J. Geophys. Res.*, 111, E09S10, doi: 10.1029/2006JE002693.

Read, P.L., and S.R. Lewis (2004), *The Martian climate revisited: atmosphere and environment of a desert planet*, Springer-Verlag, Berlin, ISBN: 978-3-540-40743-0.

Smith, M.D. (2004), Interannual variability in TES atmospheric observations of Mars during 1999–2003, *Icarus*, 167, 148–165, doi: 10.1016/j.icarus.2003.09.010.

Smith, M. D., M.-P. Zorzano, M. Lemmon, J. Martín-Torres, T. Mendaza de Cal (2016), Aerosol optical depth as observed by the Mars Science Laboratory REMS UV photodiodes, *Icarus*, 280, 234-248, doi:10.1016/j.icarus.2016.07.012.

Stamnes, K., S.C. Tsay, W. Wiscombe, and K. Jayaweera (1988), Numerically stable algorithm for discrete-ordinate-method radiative transfer in multiple scattering and emitting layered media, *Appl. Opt.*, 27, 2502–2509, doi: 10.1364/AO.27.002502.

Vicente-Retortillo, A., F. Valero, L. Vázquez and G. M. Martínez (2015), A model to calculate solar radiation fluxes on the Martian surface. *J. Space Weather Space Clim.*, 5, A33, doi:10.1051/swsc/2015035.

Warren, S.G. (1984), Optical constants of ice from the ultraviolet to the microwave. *Appl. Opt.*, 23, 1206–1225, doi: 10.1364/AO.23.001206.

Webster, C.R., P.R. Mahaffy, S.K. Atreya and the SAM Science Team (2016), Low Background Levels of Mars Methane at Gale Crater Indicate Seasonal Cycle: Updated Results from TLS-SAM on Curiosity, presented at 2016 AGU Fall Meeting, San Francisco, California, USA.

Wolff, M.J., and R.T. Clancy (2003), Constraints on the size of Martian aerosols from Thermal Emission Spectrometer observations. *J. Geophys. Res.*, 108, 5097, doi: 10.1029/2003JE002057.

Wolff, M.J., M.D. Smith, R.T. Clancy, R. Arvidson, M. Kahre, F. Seelos IV, S. Murchie, and H. Savijärvi (2009), Wavelength dependence of dust aerosol single scattering albedo as observed by the Compact Reconnaissance Imaging Spectrometer. *J. Geophys. Res.*, 114, E00D04, doi: 10.1029/2009JE003350.

Wolff, M.J., R.T. Clancy, J.D. Goguen, M.C. Malin, and B.A. Cantor (2010), Ultraviolet dust aerosol properties as observed by MARCI, *Icarus*, 208, 143–155, doi: 10.1016/j.icarus.2010.01.010.

Tables

Table 1. Discrepancy (%) between simulated and observed UVS TELRDR ratios during a shadow event on sol 1362 as a function of atmospheric opacity (τ) and dust effective radius (r_{eff}). On this sol, the opacity is ~0.7 and the retrieved dust particle effective radius is slightly above 1.5 µm.

		r_{eff} (µm)			
		0.5	**1.0**	**1.5**	**2.0**
τ	**0.1**	28.5	11.8	-3.8	-19.8
	0.5	28.2	14.2	-0.4	-15.8
	1.0	27.7	15.6	4.0	-11.4
	1.5	26.0	17.0	6.8	-7.6

Figure captions

Figure 1. (Left) Empirically derived angular response of the UVE channel (red line) and current angular response (gray line) used to obtain processed UV fluxes (in units of Wm^{-2}) available in the NASA PDS as ENVRDR data. Our empirically derived calibration function has been obtained by iteratively calculating the ratio as a function of zenith angle between measured and simulated output currents, both normalized. The angular response that we derive is consistent with that obtained by *Smith et al*. [2016]. (Right) Empirically derived field of view (FOV) of the REMS UVE channel. The region blocked by the masthead and by the mast of the rover is shown in dark blue.

Figure 2. (Top) Seasonal variability of dust aerosol particle effective radii for MY 31 (blue), 32 (black) and 33 (red). (Bottom) Seasonal variability of averaged Mastcam atmospheric opacity for MY 31 (blue), 32 (black) and 33 (red).

Figure 3. Dust aerosol particle size at the MSL landing site as a function of atmospheric opacity (τ) and solar longitude (L_s).

Figure 4. (Top) Daily UV irradiation at the TOA (black) and at the surface (red) of Gale Crater calculated using Mastcam opacities (gray) and the retrieved effective radii during the perihelion season of MY 32 and the aphelion season of MY 33 shown in Figure 2. (Bottom) Ratio between the daily UV irradiation assuming r_{eff} = 1.5 μm and the one using the retrieved radii.

Figures

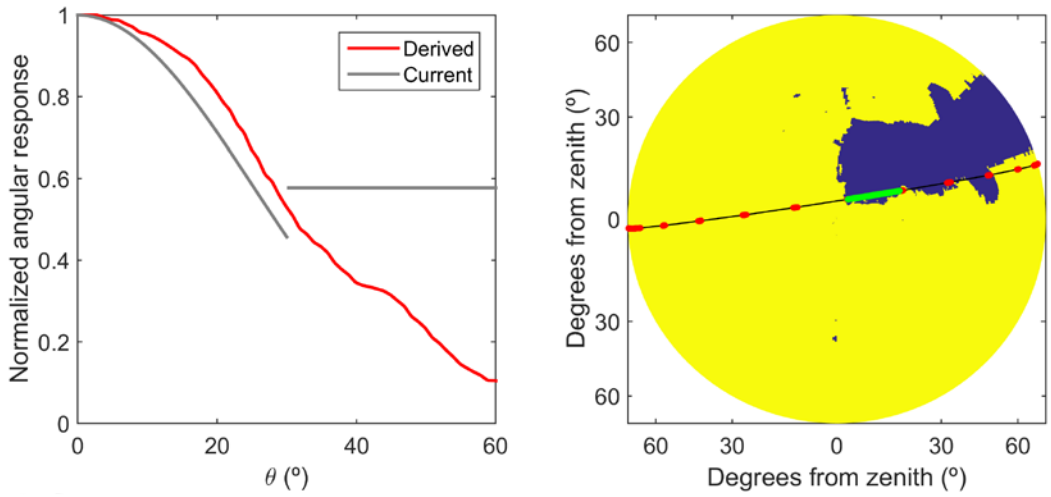

Figure 1. (Left) Empirically derived angular response of the UVE channel (red line) and current angular response (gray line) used to obtain processed UV fluxes (in units of Wm^{-2}) available in the NASA PDS as ENVRDR data. Our empirically derived calibration function has been obtained by iteratively calculating the ratio as a function of zenith angle between measured and simulated output currents, both normalized. The angular response that we derive is consistent with that obtained by *Smith et al*. [2016]. (Right) Empirically derived field of view (FOV) of the REMS UVE channel. The region blocked by the masthead and by the mast of the rover is shown in dark blue.

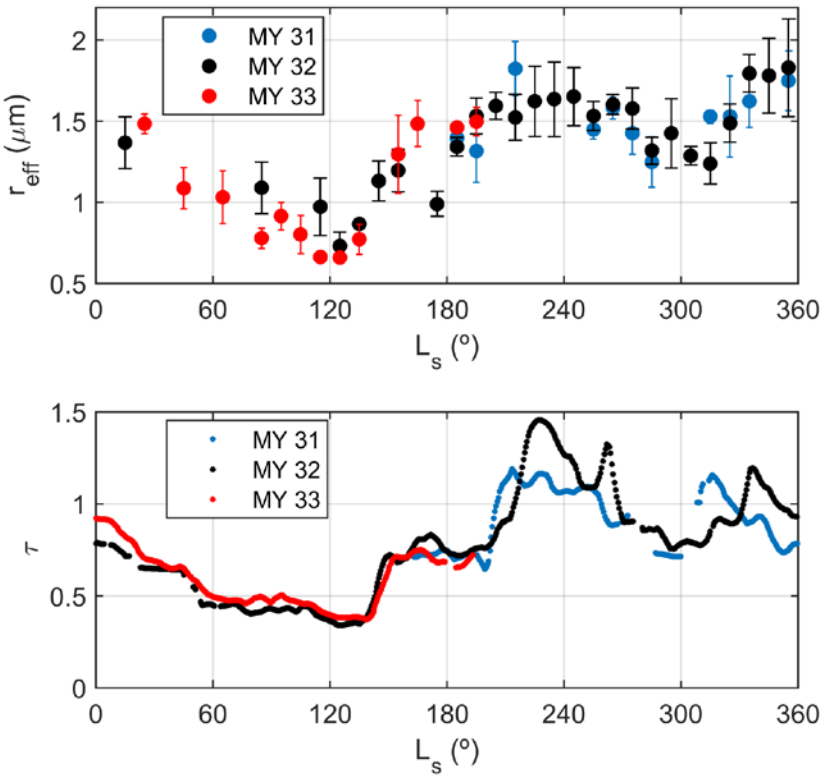

Figure 2. (Top) Seasonal variability of dust aerosol particle effective radii for MY 31 (blue), 32 (black) and 33 (red). (Bottom) Seasonal variability of averaged Mastcam atmospheric opacity for MY 31 (blue), 32 (black) and 33 (red).

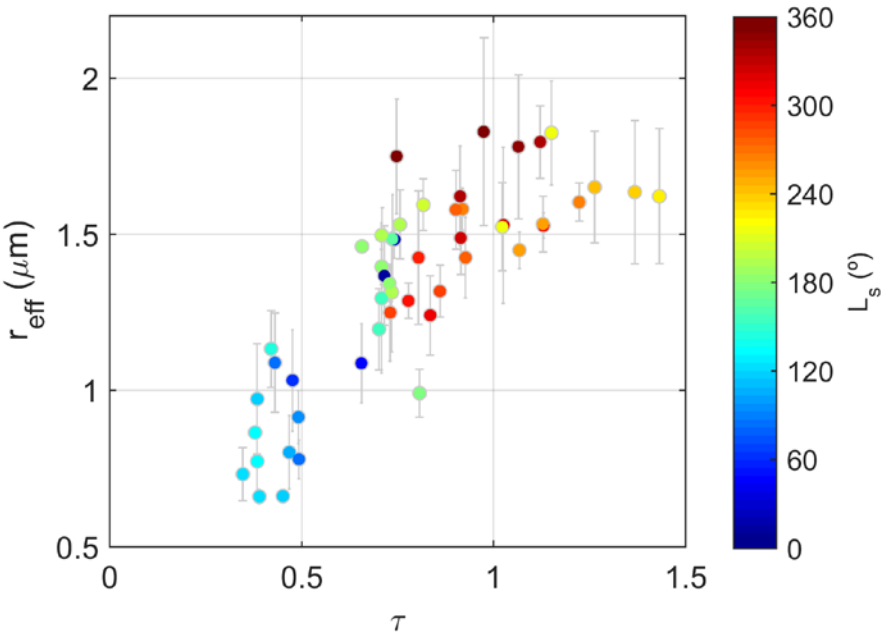

Figure 3. Dust aerosol particle size at the MSL landing site as a function of atmospheric opacity (τ) and solar longitude (L_s).

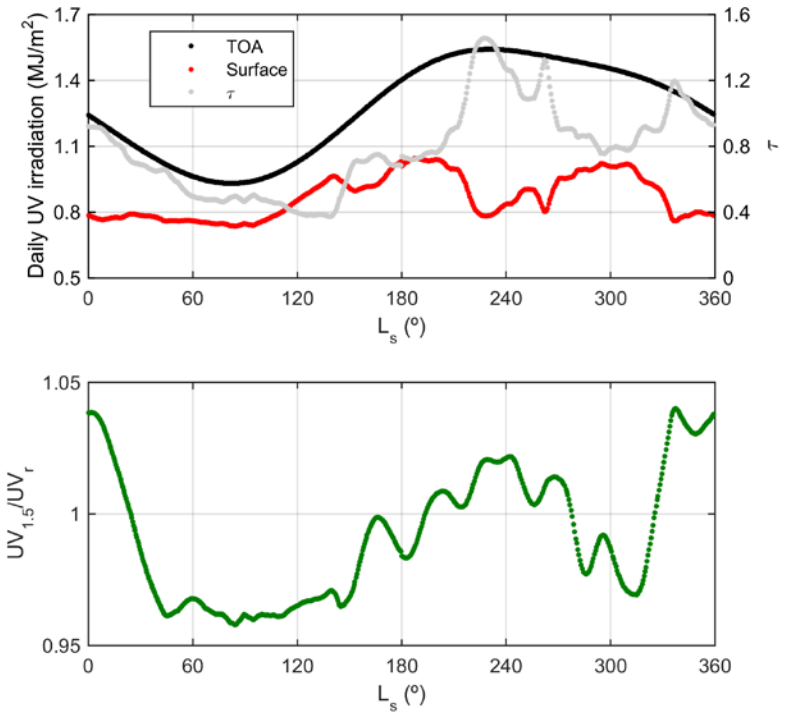

Figure 4. (Top) Daily UV irradiation at the TOA (black) and at the surface (red) of Gale Crater calculated using Mastcam opacities (gray) and the retrieved effective radii during the perihelion season of MY 32 and the aphelion season of MY 33 shown in Figure 2. (Bottom) Ratio between the daily UV irradiation assuming r_{eff} = 1.5 μm and the one using the retrieved radii.

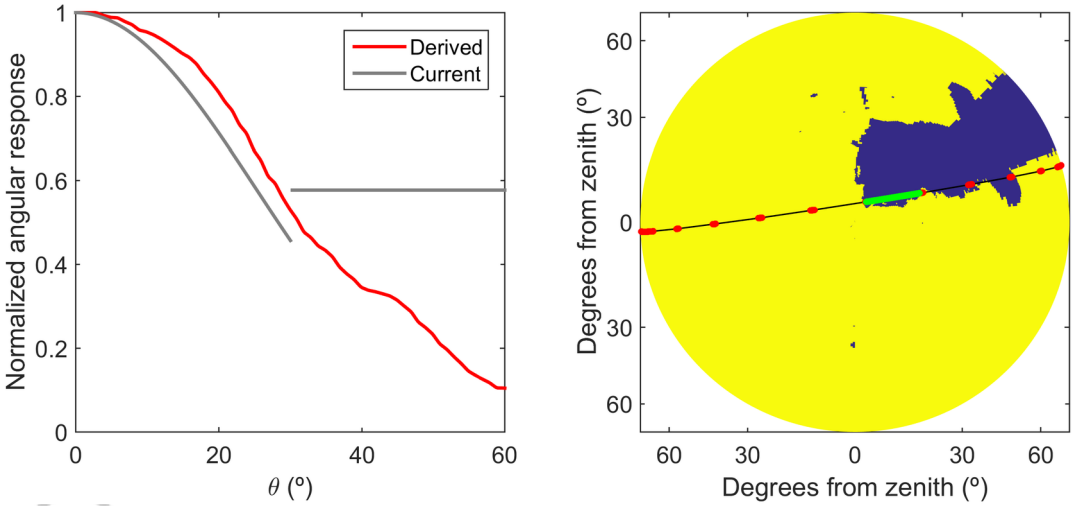

2017GL072589-f01-z-.tif

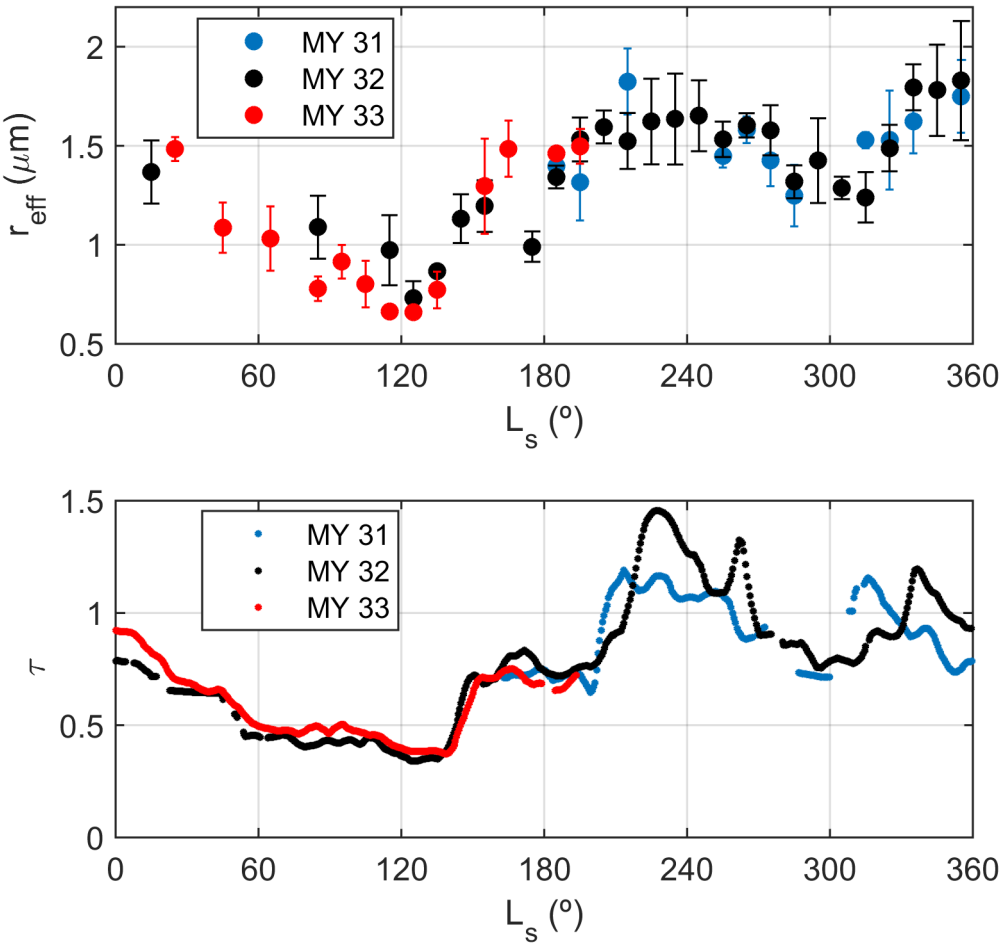

2017GL072589-f02-z-.tif

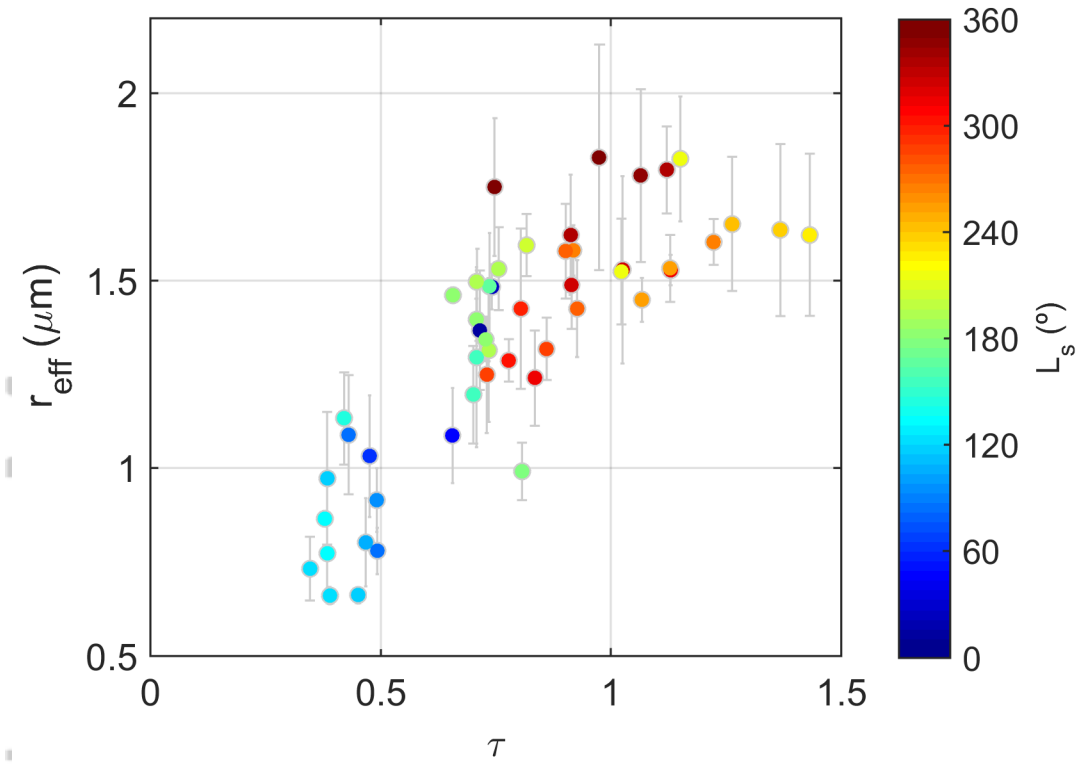

2017GL072589-f03-z-.tif

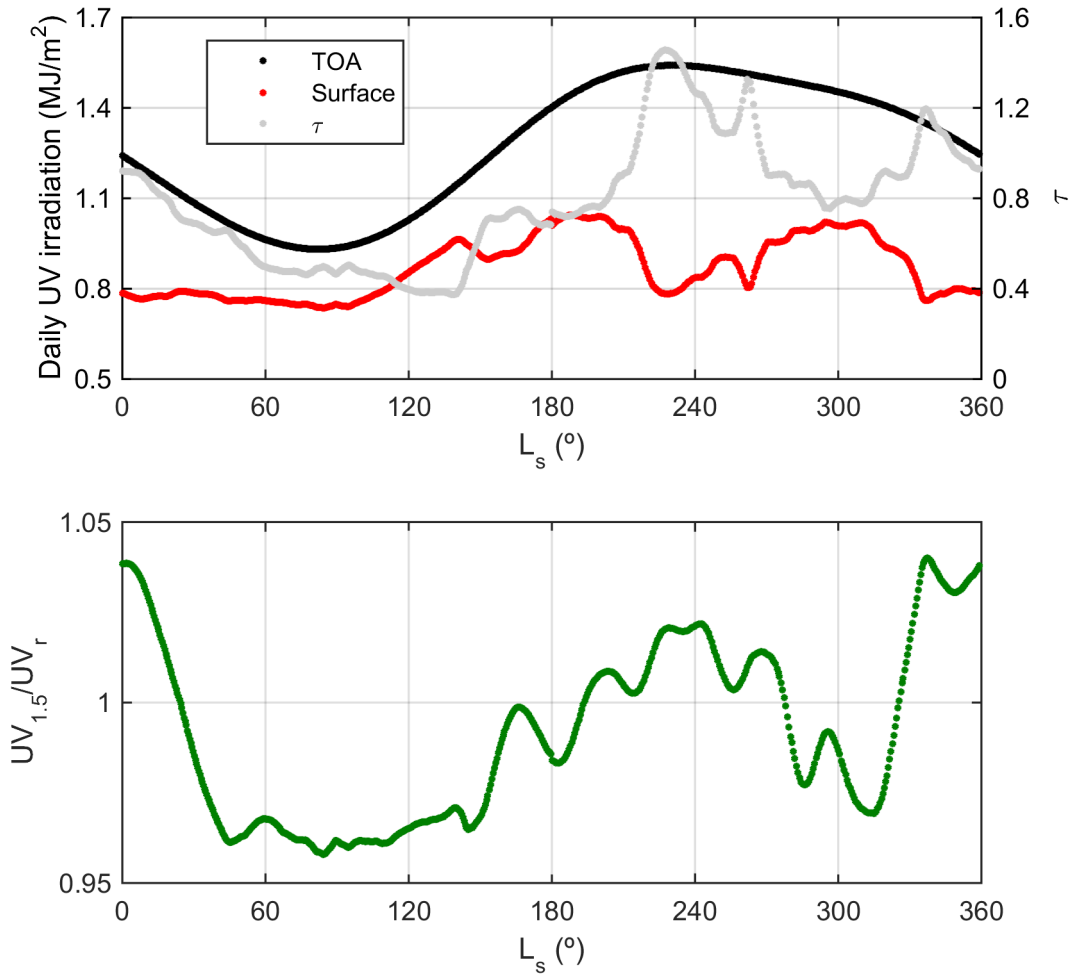

2017GL072589-f04-z-.tif